Reprinted from:

SHOCK WAVES AND HIGH - STRAIN - RATE PHENOMENA IN METALS (1981)
Edited by Marc A. Meyers and Lawrence E. Murr
Book available from: Plenum Publishing Corporation
233 Spring Street, New York, N.Y. 10013

Chapter 22

DESIGN OF UNIAXIAL STRAIN SHOCK RECOVERY EXPERIMENTS

Paul S. DeCarli
Marc A. Meyers

Poulter Laboratory, SRI-International
Menlo Park, California 94025, U.S.A.

Department of Metallurgical and Materials Engineering
New Mexico Institute of Mining and Technology
Socorro, New Mexico 87801, U.S.A.

We present an elementary introduction to the art and science of uniaxial strain-shock recovery experiments. Subjects discussed include generation of planar stress waves, design of sample recovery experiments, stress-gage instrumentation, and temperature effects. The emphasis of the present paper is practical; we hope to provide the neophyte with the basic information needed to design and interpret well-characterized shock recovery experiments.

I. INTRODUCTION

We metallurgists know that the structure and properties of a metal are strongly influenced by its thermal and mechanical history. We therefore carefully control strains, and temperatures of heat treatments, and we measure stresses, and strain rates. Our tools for studying the effects of thermal and mechanical treatments of metals have become increasingly more sophisticated, with the advent of computer-controlled testing machines, high voltage transmission electron microscopes, scanning electron microscopes, Auger spectrometers, electron-beam microprobes, and the like. However, in the area of shock-wave metallurgy, these sophisticated techniques are often used to study the results of poorly characterized experiments. The result is that, although the effects are well quantified, the causes (e.g. temperature, pressure, strain history) are substantially unknown. On the other hand, one can cite occasions on which physicists have performed superbly characterized shock loading experiments and then have thoroughly bungled the metallurgical interpretation of their results. Papers in the first category are

published in metallurgical journals; papers in the second category are published in journals of applied physics.

Obviously, we need more interdisciplinary cooperation between physicists and metallurgists. However, physicists and metallurgists often have difficulties understanding one another. This problem of interdisciplinary communication is very much like the problem faced by the American Astronauts and Russian Cosmonauts in their joint space mission. As we undoubtedly all remember, the solution to that problem was that the Cosmonauts speak only English and that the Astronauts speak only Russian.

In the first part of this paper, we discuss shock waves, shock-wave effects, and experimental design in very general and admittedly much simplified terms. We hope to introduce the physicists and metallurgists to each other's worlds, and we hope to dispell some popular misconceptions without creating any new ones. We emphasize explosive techniques; it is unlikely that our advice will be needed by the person with access to light gas gun, magnetic flyer, laser or electron-beam shock loading facilities. The second part of this paper consists of a collection of useful arts and recipes for the neophyte shock-wave experimenter.

II. GEOMETRIES

A. Plane Normal Impact

In the plane normal impact experiment a flyer plate impacts a target plate at a known velocity. If the impact is perfectly plane and if the velocity vector of the impacting plate is perfectly normal to the impact plane, then a state of pure one-dimensional strain will be produced in both flyer plate and target. This idealized geometry, depicted in Figure 1, is the usual starting point in most reviews of the physics of wave propagation.

The great advantage of this geometry is that it is relatively amenable to analysis. The stress input to the target plate is essentially a square wave having an amplitude determined by the impact velocity and relative Hugoniots of flyer and target (discussed in detail in Section IV.C.3.) However, the presence of lateral boundaries can result in a substantical alteration of the strain history of the material. This is illustrated schematically in Figure 2.

At the moment of impact the shock begins to propagate into both flyer and target. At the same moment, rarefactions originating at the lateral boundaries (points A & B) begin propagating into the target and flyer. These rarefactions cause both a rapid stress release and a transition to triaxial strain.

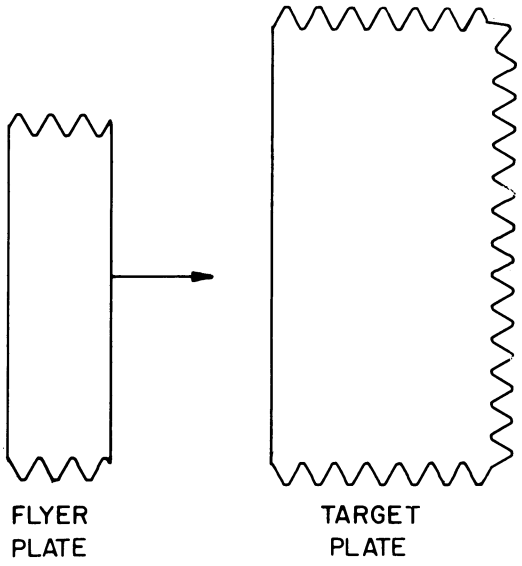

FIGURE 1. Plate impact geometry.

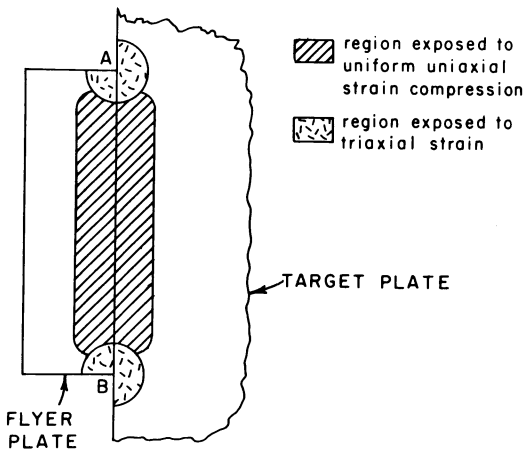

FIGURE 2. Schematic impact of a finite flyer plate on a semi-infinite target at a time after impact equal to half the shock transit time through the flyer plate thickness.

Figure 3 illustrates the conditions in this system at a later time, after release waves from the rear of the flyer plate have begun to propagate into the sample.

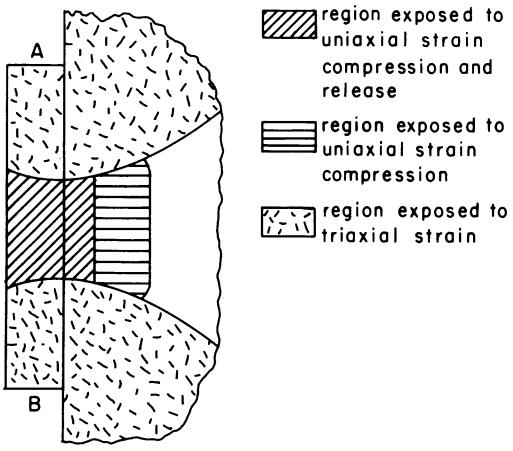

FIGURE 3. Finite flyer plate impact on semifinite target at time equal to 2.5 times the shock transit time through the flyer plate thickness.

It must be noted that the lateral release waves propagate quasi-independently of the uniaxial compression and release waves enveloping even material that has already undergone release to zero stress.

In instrumented experiments, observations are generally confined to the region (in time and space) of one-dimensional flow. Through use of lateral momentum traps is discussed later in Section IV.F., it is possible to actually recover samples that have been subjected macroscopically to pure uniaxial compression plus release, or to uniaxial compression followed by uniaxial tension and then release.

Only the leading edges of the shock and rarefaction fronts are shown in Figures 2 and 3. Neither the shock nor rarefaction fronts are as simple as these figures imply. Furthermore, we have completely ignored effects of wave interactions occurring later in time.

B. Plane Inclined Impact

In this geometry, illustrated in Figure 4, the impact is perfectly planar, but the velocity vector of the flyer plate is *not* normal to the plane of impact.

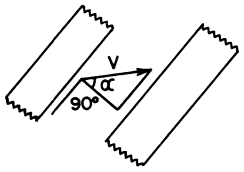

(a) Inclined impact geometry, velocity vector (V) inclined at angle α to plate normal.

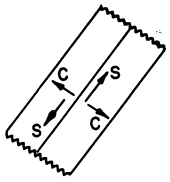

(b) Impact generation of compression (C) and shear (S) waves.

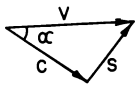

(c) Velocity vector decomposed into compressive component ($C = V \cos \alpha$) and shear component ($S = V \sin \alpha$).

FIGURE 4.

Note that the impact velocity can be decomposed into compressive and shear components. If one wishes to calculate the impact stress using the impedance-match method of Sections IV.D., the "impact velocity" that must be used is the compressive (normal) component of the impact velocity vector. The plane inclined impact geometry is one-dimensional. Since the shear wave propagates more slowly than the compressional wave, this geometry permits study of the propagation of shear waves in a uniaxially compressed material. This technique is very new and is just beginning to yield results, both in instrumented and recovery experiments.

C. Non-Planar Impact

The non-planar impact, illustrated in Figure 5, is another method of producing both compressive and shear waves in a target.

The disadvantage of this technique is that the flow is two-dimensional and complicated by wave interactions in target and flyer. In principle, modern computer codes are capable of detailed two-dimensional flow calculations. In practice, the accuracy of the code calculation is dependent on knowledge of material properties under combined compression and shear. Many experiments with non-planar

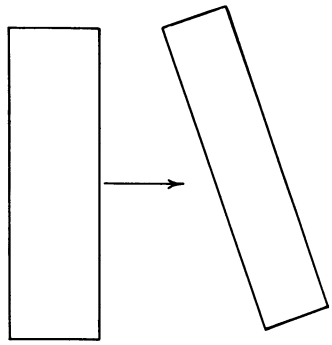

FIGURE 5. Non-Planar Impact.

impacts are accidental, i.e., the experimenter had intended to achieve a planar impact. The non-planar impact is the standard geometry for explosive welding. Jetting and other two-dimensional flow phenomena at the interface serve both to break up the oxide layer and to heat a thin layer of material to a sufficiently high temperature to permit welding. Regions of a flyer plate in which the impact deviates substantially from planarity often show the familiar "ripple" pattern.

III. EXPERIMENTAL TECHNIQUES

A. Laser and Electron-Beam Loading

These techniques are basically similar. A large flash of energy, either laser or electron beam, is deposited upon the surface of the target. The rapid expansion of this surface region results in a shock wave moving into the target. The great advantage of these techniques is that the shock wave initiation is essentially simultaneous over the area irradiated. However, the area irradiated is generally limited by the power available to less than 10 cm^2. Furthermore, the distribution of energy over the irradiated area is frequently non-uniform, i.e., the peak stress varies over the

irradated area. The stress pulses are short of the order of 0.1 μs duration, and therefore attenuate rapidly.

One of the major problems associated with electron-beam and laser pulse loading is diagnostics; it is very difficult to accurately determine the stress profile induced in a target in a given experiment. These measurement difficulties stem from the fact that the production of a laser or electron-beam pulse is accompanied by an intense burst of electromagnetic noise. It is extremely difficult to shield stress instrumentation systems (e.g. piezoresistive, piezoelectric, laser interferometric) from pickup of this noise, and it is frequently the case that the stress signals are completely obscured by noise. In general, stress measurements in electron-beam and laser pulse experiments are made at a plane 3 to 6 mm behind the front surface of the target. The resultant time delay (the shock-wave propagation time) permits the prompt electrical noise picked up by the signal cables to decay substantially (in an electrically well-damped system) before onset of the stress signal.

It must be emphasized, however, that the observed stress pulse at the rear surface of a 4 mm-thick sample could differ substantially in amplitude, shape, and width from the stress pulse at 1 mm depth.

B. Exploding Foil Techniques

In this technique a thin metal foil is vaporized or exploded by a pulse of very high current. A thin dielectric plate adjacent to the foil is accelerated to high velocity by the foil explosion and, after a short free flight, impacts the target. In principle, the impact should result in the production of a short-duration flat-topped stress pulse in the sample. However, a slight deviation from planarity of impact can result in a substantial decrease in the peak stress and a corresponding increase in pulse width, as shown in Figure 6. Only the total impulse is the same for planar and non-planar impacts.

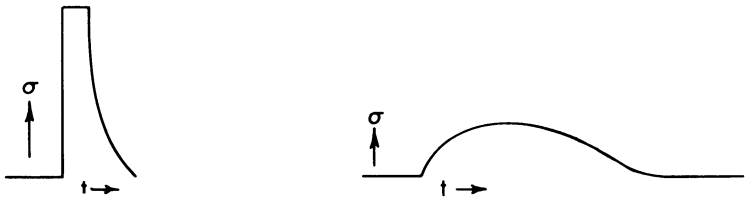

FIGURE 6. Effect of planarity on stress profiles produced by impact of thin flyers; (a) planar impact; (b) non-planar impact.

As in the case of laser and electron-beam experiments, exploding foil experiments produce substantial electrical noise, and electronic instrumentation is difficult.

C. Gun Techniques

The gun technique simply entails the impact of a target with a flat-nosed projectile. Either a propellant (e.g., smokeless powder) or compressed gas may be used to accelerate the projectile. In general, compressed gas guns are preferred on the basis of operating convenience and predictability of impact velocity. In order to avoid driving a strong air shock ahead of the projectile, it is necessary to evacuate the gun barrel to a pressure of 2-5 Pa. Blow-by of the driver gas is minimized through use of teflon-coated O-ring seals on the projectile. The head of the projectile may consist of a flyer plate backed up by low-impedance foam or honeycomb, as in Figure 7. The impact pressure pulse length is governed by the thickness of the flyer plate, by the diameter of the flyer plate and by the shock and release wave velocities in both flyer plate and target materials, as discussed in Section IIA.

Light gas guns may be used in an ordinary laboratory setting; since the barrel and debris collection chamber are evacuated, the noise is minimal. The projectile impact velocity is routinely measured, and, in most experiments, the impact planarity is measured, as well. Techniques for performing recovery experiments are well established, and, in general, gas gun recovery experiments permit a narrow definition of the stress-strain history of the sample.

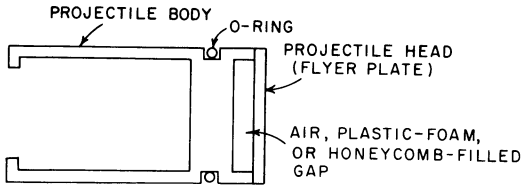

FIGURE 7. Cross-section of light gas gun projectile.

For experiments with very thin flyers, one is generally concerned that the flyer will be bowed during projectile acceleration. However, one can then place the thick target on the projectile head and impact a stationary thin "flyer".

Recently, the SRI 65 mm diameter light gas gun has been modified by cutting a straight keyway in the barrel. A matching key on the projectile engages the keyway and projectile rotation is prevented. With projectile non-rotation assured, the gun can be used for plane inclined impact experiments.

The impact velocity range accessible to single stage gas gun experiments ranges to about 1.5 km/sec and projectile diameters (the diameter of the plane impact region) are commonly in the range of 65 mm to 100 mm. Corresponding peak pressures and durations for symmetrical impact of common metals are a few hundred kbar (a few tens of GPa) and a few microseconds. The initial cost of even a modest light gas gun facility is comparable to that of an electron microscope.

IV. THE (HIGH EXPLOSIVE) SYSTEMS

Explosively-driven systems are the technique requiring least capital investment and, hence, best suited for start-up of a shock-loading program. It is assumed, of course, that the user is familiar with the safety requirements in the use of explosives. It is obvious that great care should be exercised in the handling of explosives; this is especially true in the case when new systems are being tested. Different experimental arrangements have been developed throughout the years to transform a point detonation (produced by a detonator) into a plane detonation. Several of these will be reviewed here and it will be shown how they can be designed. First, the point detonation is transformed into a line detonation by means of a line-wave generator. Then, the line detonation is transformed into a plane detonation by means of a plane-wave generator.

A. Line and Plane-Wave Generators

1. Line-Wave Generators

Among the various systems designed, the perforated triangle and the geodesic surface are the most common ones. The perforated triangle is initiated at one of the vertices by a cap and small booster charge. The detonation front has to pass between the holes, and the curved trajectory D_1 is the same than the trajectory at the edges, D_2 (Figure 8). Hence, the wave front is linear. The diameter and spacing of the circles are chosen in such a way that the above conditions are met. Line-wave generators are commercially available from DuPont but can be easily fabricated by making two steel dies with the appropriate hole pattern; the sheet explosive is placed between the dies and a punch is used to perforate the explosive. Typical dimensions are A = 0.25" (0.64 cm), B = 0.3" (0.76 cm). These DuPont line-wave generators were tested at

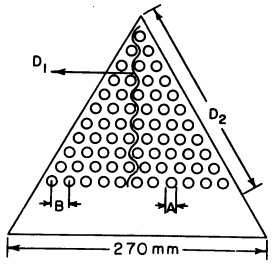

FIGURE 8. Triangular line-wave generator.

Stanford Research Institute (1) and it was found that there was a variation in ~0.5 μs in the arrival time of the wave on the side opposite to the detonation initiation apex; this corresponds to a deviation from a straight line of about 3.4 mm.

One geodesic surface consists of a sliced cone covered by sheet explosive; it is shown in Figure 9. It can be manufactured from a wooden cone (light wood) and with cuts made at 30°, as shown in Figure 9. It should be noticed that the bottom surface is not covered with explosives. It provides a detonation front that is as regular (if not more) than the perforated line-wave generator. One of its advantages is that one can scale it up and down in size. There are other types of line-wave generators; one of them is discussed by Kestenbach and Meyers (2); additional ones are presented by Benedick (3).

2. Plane Initiation

In order to transport a planar shock front to the flyer plate or to the system, the point or line detonation has to be transformed. These systems will be discussed.

a. Explosive Lens Figure 10 shows one of the possible designs for an explosive lens. The detonator transmits the front to two explosives which have different detonation velocities. The inside explosive has a detonation velocity, V_{d_2} lower than the outside one. The angle θ is such that:

$$\sin \theta = \left(\frac{V_{d_2}}{V_{d_1}} \right) \qquad [1]$$

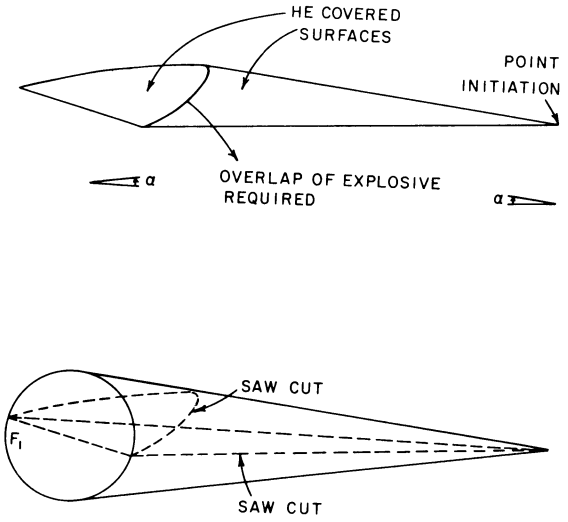

FIGURE 9. (a) Geodesic surface, (b) Schematic indication of how a geodesic surface can be cut from a light-wood cone ($\alpha = 30°$).

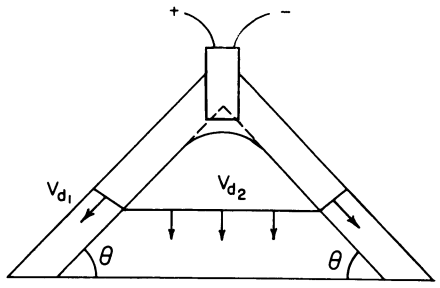

FIGURE 10. Conical explosive lens.

The apex of the cone is not exactly straight; a certain curvature is introduced to compensate for initiation phenomena (the steady detonation velocity is not achieved instantaneously) and for the fact that the initiation source is not an infinitesimal point source. Because of these and other complications, such as the requirement for precision casting of explosives, fabrication of explosive lenses is best left to specialists.

b. Mousetrap Plane Wave Generator The mousetrap assembly is frequently used for metallurgical work. Figure 11 shows a common set-up. Two layers of Detasheet C-2 (2 mm thick each) are placed on top of the 3 mm thick glass plate tilted at an angle α to the main charge. The detonation of the explosive will propel the glass into the main charge; all glass fragments should simultaneously hit the top surface of the main charge, resulting in plane detonation. It has been experimentally found that one layer of Detasheet C-2 does not propel the fragments with a velocity high enough to initiate the main charge, if it is Detasheet. The angle α is calculated from the velocities of detonation and fragments, V_d and V_f, respectively. The velocity of fragments can be calculated using the Gurney equation, in Section IV.C.3. For the system shown in Figure 11, it has been found that $\alpha = 11°$ provides a good planarity. The extremity of the line-wave generator should be inserted between

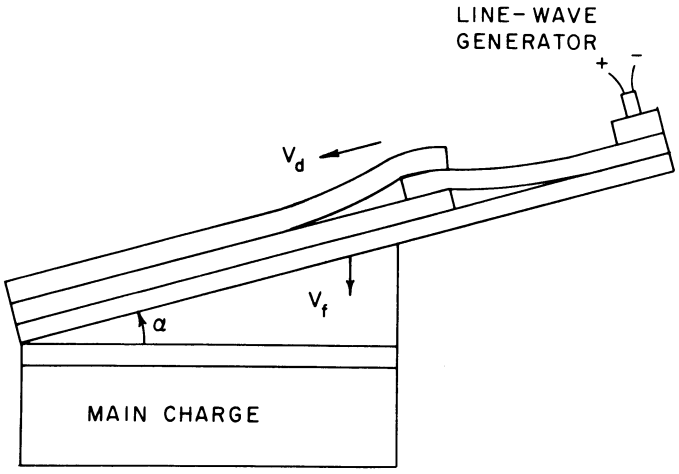

FIGURE 11. Mousetrap plane-wave generator showing detonation velocity, V_d, and fragment velocity, V_f.

the two plane-wave generator sheets. Usually the glass piece is cut so that the line-wave generator, booster, and plane-wave generator are glued to it. Metal plates can also be used instead of glass.

B. Plane-Initiated Contact Explosives

The detonation front in the explosive is preceded by a shock wave. Appendix A (p.1033, this volume) describes the process of detonation in greater detail. When the shock front of the explosive reaches the explosive-metal interface it will propagate into the metal. Both shock velocity and peak pressure will be different, and calculations have to be conducted to determine the values. The well-known impedance-matching technique is used to calculate the interface pressure. This technique is explained for plate impact in Section IV.D. A similar approach is used here. The pressure vs. particle velocities for the metal and explosive are shown in Figure 12. The pressure P_{cj} shown in the plot is the Chapman-Jouguet pressure. The pressure at the shock front on the explosive (von Neumann Spike) will not be considered, since it attenuates in the first fraction of one mm into the metal. The impedance-matching technique is based on the requirements that pressure and particle velocity be continuous across an interface. Hence, the pressure in the metal will be determined by the intersection of the reflection Hugoniot of the explosive passing through (P_e, U_{pe}) and the transmission Hugoniot for the metal. This

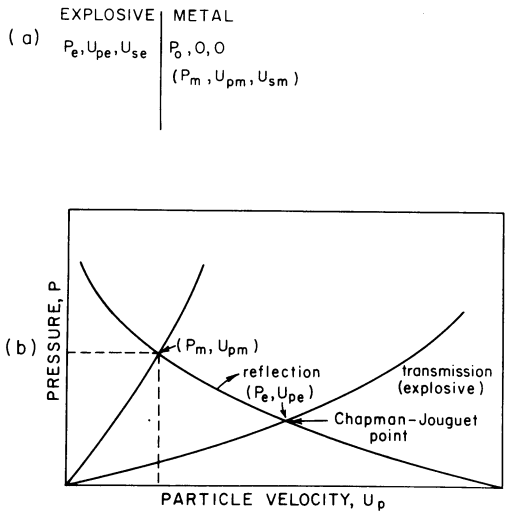

FIGURE 12. (a) Pressure, particle velocity and shock velocity at the two sides of an explosive-metal interface. (b) Pressure vs. particle velocity plot for metal and explosive; the latter passes through the Chapman-Jouguet point.

is explained in greater detail by Duvall and Fowles (4) and Jones (5). In Figure 12, this corresponds to the pressure P_m, and particle velocity U_{pm}. Figure 13 shows a reflection Hugoniots for a number of explosives. They all pass through the Chapman-Jouguet state for the respective explosive.

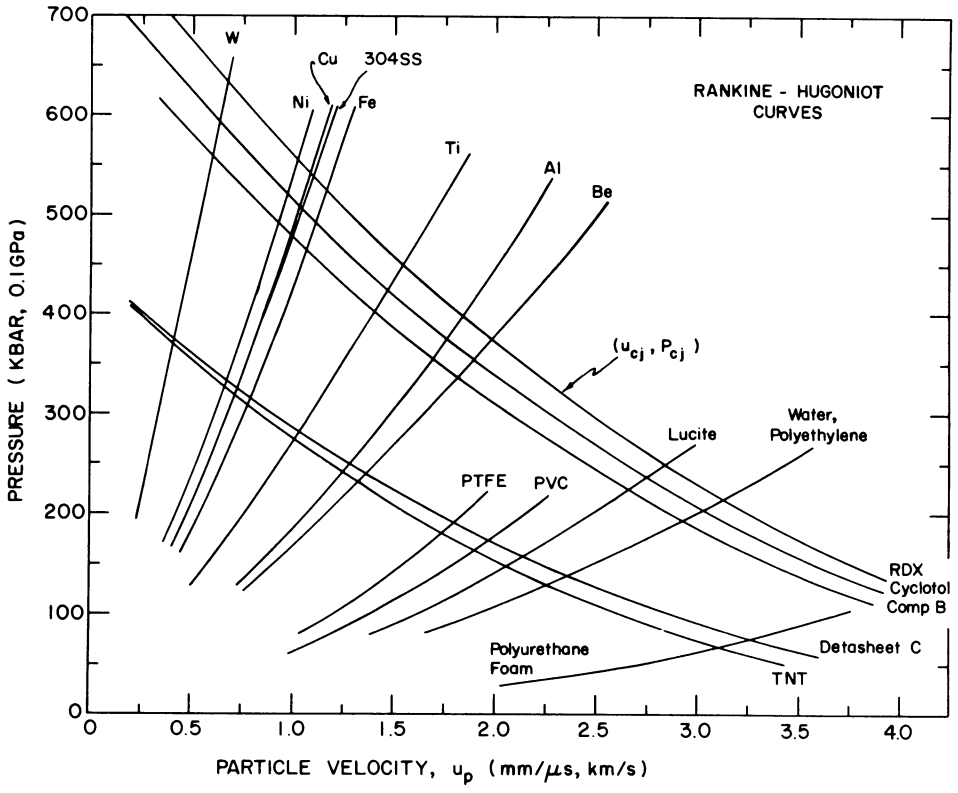

FIGURE 13. Shock waves induced in various materials by normally-incident plane detonation waves (after reference 27).

Without further qualification, it is meaningless to speak of the duration of the pressure pulse generated in a metal sample by the detonation of explosive-in-contact; the peak pressure determined by the impedance matching technique immediately begins to decay as the detonation products of the explosive expand. As the shock wave progresses through the metal sample, rarefactions originating at the explosive-metal interface overtake the shock and reduce the shock pressure. One must not be led astray by the fact that most discussions of shock-wave properties concentrate on the ideal one-dimensional (no lateral boundaries) geometry. In fact, the pressure pulse shape will be drastically modified by rarefactions originating at lateral boundaries, as indicated schematically in Figure 14.

Contact-explosive geometries are very useful for practical purposes, such as shock-hardening of Hadfield steel or austenitic stainless steels. However, the metallurgist must be warned that the results of recovery experiments performed with contact explosives are likely to be subject to ambiguities of interpretation. For example, one may not be able to determine whether an observed phenomenon is the result of a *short-duration high pressure portion or of a longer duration, lower pressure, portion of the triangular stress wave.*

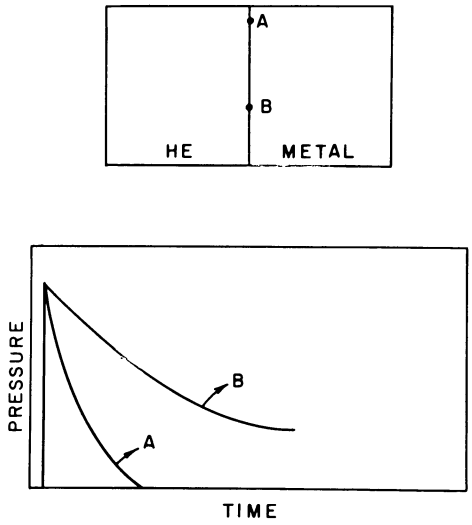

FIGURE 14. Pressure-time profiles at two positions (A and B) within a metal-explosive interface.

C. Flyer-Plate Geometry and Design

The normal impact of a flyer plate on a target generates a pressure pulse that is characterized by a sharp pressure rise, a region in which the pressure is constant (pulse duration) and a gradual return of the pressure to zero. This is schematically shown in Figure 15. The shape of this pressure pulse changes as it travels throughout the material. The release wave has a higher velocity than the shock front and gradually overtakes it. The three points A, B, and C on Figure 15 (a) (at increasing distances from the impact interface) are subjected to different pressure pulses (Figure 15 (b). As the release wave overtakes the shock wave the pulse duration decreases; at C it is already zero, and the peak pressure is reduced from its initial value. The distance-time plots of Figure 15 (c) and (d) show how the flyer-plate thickness and material determine the wave parameters. These types of plots are commonly used to characterize the progress of shock waves throughout a material. Point O marks the instant and position of impact Compressive waves propagate into the flyer plate and the target. When the compressive wave in the flyer reaches the rear surface, the compressed flyer plate becomes free to expand; a rarefaction wave moves back through the flyer plate. In the language of the shock-wave physicist, the compression wave reflects as a rarefaction. The rarefaction wave travels at the speed of sound in the compressed material. This velocity is higher than the shock velocity. However, as the material expands, the sound speed decreases. For this reason, the pressure decay on rarefaction is spread out in time, in comparison with the sharp pressure discontinuity at the shock front. When the leading edge of the rarefaction originating at P_1 reaches P_2, the flyer-target interface, it propagates into the target. If flyer and target are the same material, there are no interactions of the release wave with this interface. If flyer and target are of different materials, of substantially different shock impedance, the rarefaction wave does interact with the flyer-target interface; both flyer and target undergo a succession of reflected shocks and rarefactions. As in the case of contact explosive experiments, the complexity of the stress history makes it difficult to determine cause-and-effect relationships. For this reason, symmetrical impact experiments, in which both flyer and target are the same material, are generally preferred.

Upon reaching the rear surface, the shock wave in the target is reflected as a rarefaction. When the rarefaction originating at the rear surface of the target meets the rarefaction originating at the rear surface of the flyer, a tension results. This tension persists until the rarefaction waves have propagated to the rear surface and flyer plate-target interfaces and returned as reflected recompression waves. Note that a tension can not propagate across an unbonded interface; this fact is the basis of the momentum-trapping principle illustrated in Figure 15 (d).

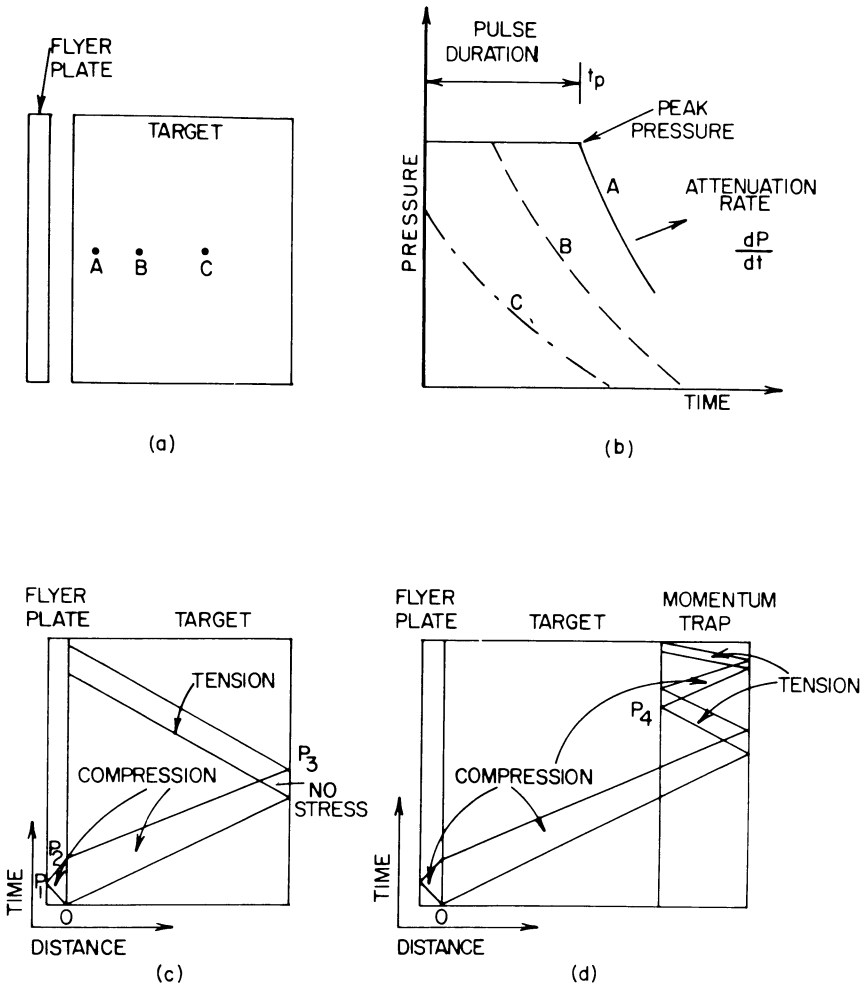

FIGURE 15. (a) Points A, B, and C at increasing distance from target-flyer interface. (b) Change in shock-pulse shape as it enters the material. (c) Distance-time plot showing pressure pulse reflecting itself at back surface. (d) Same as (c) but with a momentum trap "trapping" reflected tensile pulse.

It is important to fully characterize a pressure pulse traveling through a metal. In order to do this, it is necessary to specify the peak pressure, P, the pulse duration, t_p, and the rarefaction rate dP/dt = P. These are, in turn, dependent upon the flyer plate velocity, v_p, thickness, t, and material. Sections IV.C.1. through IV.C.3., and Sections IV.D.1. through IV.D.3. will instruct the prospective shock-loader on how to correctly perform these calculations.

1. Inclined Plate

Figure 16 (a) shows schematically the inclined-plate geometry. It is preferred over the parallel plate (described in the next section) geometry for pressures up to 10 GPa because the calculations can be applied without great error. In essence, this is the same as the mousetrap plane wave generator discussed in Section II. B. Instead of using a glass plate to initiate an explosive, one uses a metal plate to directly impact the target. The angle of inclination of the plate is chosen so that impact of the plate with the target will be plane (6). Both Duvall and Fowles (4), and Nordstrom, et al., (6) recommend its use for lower pressures. The

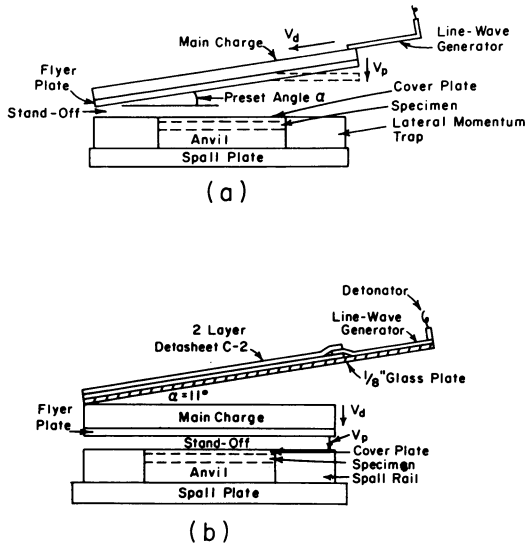

FIGURE 16. Shock-loading systems using HE (after reference 27), (a) Inclined-plate geometry, (b) Parallel-plate geometry with mousetrap plane-wave generator.

line-wave generator initiates the explosive at the top portion of the plate. The explosive propels the plate downwards. The angle α can be determined from the detonation and plate velocities V_d and V_p, respectively. One has:

$$\sin \alpha = \frac{V_d}{V_p} \qquad [2]$$

The plate velocity is calculated using the Gurney equation, that will be discussed in detail in Section IV.C.3.

2. Parallel Plate

This is the standard assembly used for medium and high-pressure events; a typical system with a "mousetrap-type" plane-wave generator is shown in Figure 16 (b). Detonation is started simultaneously over the whole top surface of the main explosive charge. Once detonation is completed the flyer plate is accelerated downwards. The edges of the flyer plate will lag behind, and only the central portion (about half the area) of the flyer plate will produce plane impact. The angle α in the mousetrap is calculated by the equation presented in Section IV.C.1, substituting V_f for V_p.

3. Calculation of Impact Velocity

The simple equation proposed by Gurney (7-9) in 1943 has proven to be remarkably reliable. It was initially applied to determine the velocity of fragments from bomb shells and grenades. The basic assumption behind the Gurney equations is that the contribution to the kinetic energy of the fragments made per unit mass of explosive is the same independent on the size of the shell. Hence, the important ratio as a function of which the fragment velocities are calculated is the ratio between the mass of explosive (c) and the mass of metal (m). The derivation of the original Gurney equation is very simple. The chemical energy of the explosive is equated to the kinetic energy ($1/2\ mv^2$) of the fragments and detonation products after the explosion. From this relationship Gurney was able to obtain v for various bomb, shell, and grenade geometries. For the plate geometry used in shock-loading assemblies, the Gurney equation is:

$$V_p = \sqrt{2E}\left[\frac{3}{1 + 5\left(\frac{m}{c}\right) + 4\left(\frac{m}{c}\right)^2}\right]^{1/2} \qquad [3]$$

V_p is the plate velocity; E is the energy of the explosive, per unit mass; m and c are the masses of the metal and explosive per unit area respectively. From the densities and thicknesses of metal plate (P_m,t) explosive (P_c,t_c) it is possible to calculate the ratio m/c:

$$\frac{m}{c} = \left(\frac{\rho_m}{\rho_c}\right) \cdot \left(\frac{t_m}{t_c}\right) \qquad [4]$$

The Gurney energy of the explosive, E, is dependent upon the angle between the detonation front and the plate because the escape path of the detonation products is different for the different geometries. Hence, one has to use different Gurney energies for the inclined plate and parallel plate geometries. Appendix A (p.1033, this volume) provides an overall description of the detonation of an explosive as well as tabulated data on the explosive density ρ_c, detonation velocity, V_d, and Gurney energies for normally incident detonation fronts for the most important explosives; for grazing incidence, one has to calculate the energy using Equation A-10, in Appendix A. Appendix E (p.1057, this volume) provides a very convenient nomograph of the Gurney formula.

In spite of the fact that more complex formulations have been proposed for the velocities of fragments and plates, the original Gurney equation has been proven to be very reliable (10,11). In a systematic investigation conducted at Stanford Research Institute, Roth (11) concludes that the simple Gurney theory is as good as the more sophisticated ones; its only limitation is that it is not applicable to situations before the terminal conditions are achieved and when m/c tends to zero. Figure 17 shows the comparison between

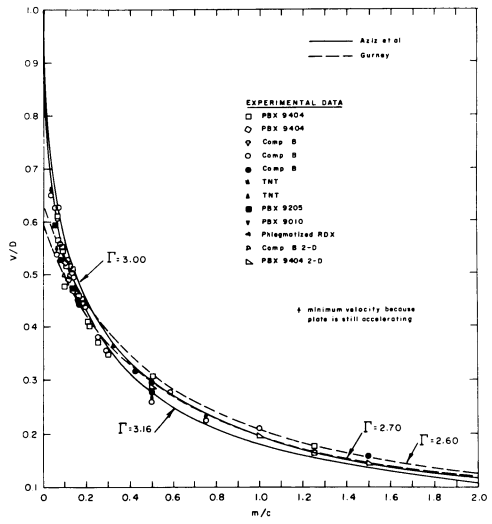

FIGURE 17. Comparison of the prediction of Gurney formula (– – –) for flyer-plate velocities at various m/c values with experimental results and more complex equation (——) (after ref.11).

experimental and theoretical plate velocities. It can be seen that the Gurney equation compares well with experimental results for m/c values above 0.1. The parameter Γ is related to the equation of state of the detonation products and is included in the tabulated Gurney energies (see Appendix A, where it is designated by γ).

It is very important to notice that the Gurney equation only predicts the terminal velocity of the plate; actually, it accelerates from its initial rest position. Enough stand-off distance has to be left between the flyer plate and the target. This is treated in Section IV.E.

D. Calculation of Shock-Wave Parameters

1. Calculation of Peak Pressure

The pressure imparted on the system by the impact of a flyer plate is calculated by a technique called *impedance matching*. The Rankine-Hugoniot equation relating the pressure, P, and particle velocity, Up, is used.

The physical basis of the impedance matching technique is the requirement that particle velocity and pressure be continuous across the collision interface. If U_p^F and U_p^T are the particle velocities in the flyer plate and target interfaces, respectively, one has:

$$V_p - U_p^F = U_p^T \quad \text{and} \quad V_p = U_p^F + U_p^T \qquad [5]$$

Prior to impact one has $V_p = U_p^F$ and $U_p^T = 0$; after impact U_p^F decreases, allowing for a non-zero U_p^T. The impedance-matching technique has a simple graphical solution, shown in Figure 18. The $P - U_p$ curves for both target and flyer plate are shown starting at the origin (when pressure is zero, so is the particle velocity). Taking the $P - U_p$ curve for the flyer plate, rotating it by 180° and passing it through the new origin $(V_p,0)$, one obtains the reflection curve. It will intersect the target curve at (U_p,P). Notice that at this point one has:

$$P^F = P^T \qquad [6]$$

and

$$U_p^T + U_p^F = V_p \qquad [7]$$

These are the continuity conditions and point (U_p,P) satisfies the conditions of both flyer and target plates. Appendix C (p. 1045, this volume) provides information from which it is possible to construct $P - U_p$ curves for a whole range of materials. The particle

velocities, U_p, are tabulated as a function of pressure (2.5 GPa intervals, up to 60 GPa) for a number of these materials in Appendix F (p.1059, this volume). All one has to do is to make the pressure-particle velocity plots on transparent paper; one marks the point $(V_p,0)$ on the abscissa of the target and inverts the plot for the flyer material, positioning its origin at $(V_p,0)$. The intersection of the two curve gives the pressure. If both flyer plate and target are the same the task is simplified since one will have:

$$U_p^T = U_p^F = U_p = \frac{V_p}{2} \qquad [8]$$

There is no need for tracing, and a line passing through point $(V_p/2,0)$ parallel to the P axis will intersect the P - U_p curve at the pressure.

In the case the Hugoniot curve for an alloy is required, the procedure recommended in Appendix D should be used. Then, applying the equations in Appendix C (p.1045, this volume), one obtains the desired data. A detailed description of the possible ways of interpolating Hugoniot curves for alloys from the pure elements is also given by McQueen, et al., (12).

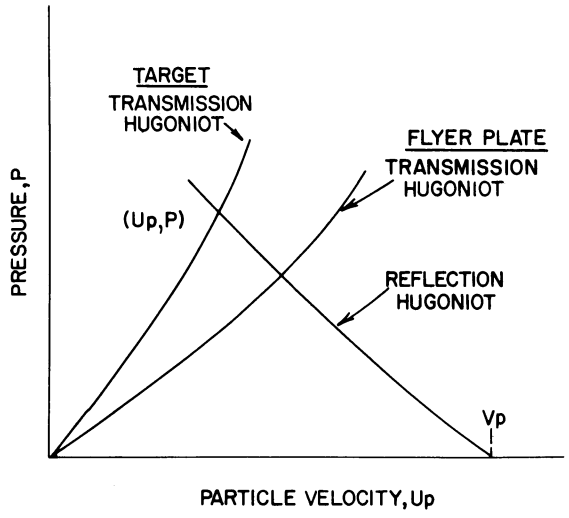

FIGURE 18. Pressure vs. particle velocity for both the target and flyer plate; for the flyer plate one uses the reflected curve passing through V_p.

2. Calculation of Peak-Pressure Duration

The initial duration of the pulse traveling through the metal is usually determined by the flyer-plate thickness. However, if the flyer plate is thicker than the target and no spall plates are used, the thickness of the target can establish the pulse duration. The former situation will be analysed first.

The calculation of t_p when a flyer plate impacts a target plate in a parallel manner can be understood from Figure 19, where distance is plotted against time. When a flyer plate of thickness t^F and impact velocity V_p collides with a specimen or target plate, particles are accelerated in the positive direction (Figure 19) in the target, thereby producing a shock moving to the right into the target. Conversely for the flyer, particles are decelerated in the positive x direction, or accelerated in the negative x direction, producing a shock wave moving to the left, into the plate, away from the collision interface. When the flyer and target are the same material, the flyer plate velocity is partitioned equally between the two, so that

$$V_p = U_p^F + U_p^T = 2\ U_p \qquad [9]$$

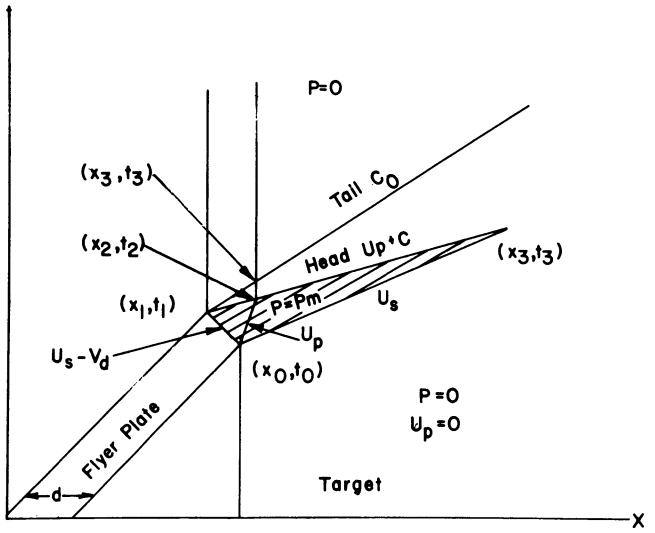

FIGURE 19. Distance-time plot of impact of flyer plate on target showing decrease of pulse duration as pressure pulse advances into target.

where U_p^F is the particle velocity of the shock wave reflected into the flyer plate. The time taken for the reflected shock to reach the front face (i.e., explosive flyer interface) of the flyer is given by

$$T_1 = t_1 - t_o = t^F/U_s \quad [10]$$

The shock wave is then reflected as a rarefaction wave at the free surface and this releases the pressure as it returns toward the collision interface at a relative velocity corresponding to the velocity of sound, c, in the compressed medium of thickness (ρ_o/ρ) t^F in a time.

$$T_2 = t_2 - t_1 = \rho_o t^F/\rho c \quad [11]$$

This results from the fact that the collision interface itself and all of the flyer material is moving at velocity U_p. If one were considering stationary material ahead of the shock front, then the rarefaction wave would approach it at a velocity $c + U_p$.

Effectively, then, the pulse duration at the front face of the target (collision interface) is

$$t_p = T_1 + T_2 = t^F\ (1/U_s + \rho_o/\rho c) \quad [12]$$

The values of U_s, U_p, and c are tabulated in Appendix F (p. 1059, this volume) for a number of metals.

If one wants to determine the pulse duration in a simpler and less rigorous manner, one simply applies the equation:

$$t_p = \frac{2t^F}{U_s^F} \quad [13]$$

It is worth pointing out that if a series of experiments at different pressures is conducted by maintaining the same flyer plate thickness and material, the pulse duration will change. This is illustrated in Figure 20, for an AISI 304 flyer plate impacting a titanium target. The pulse duration varies by ± 10 pct as the pressure is varied over a 20 GPa range (13). This pulse length variation is due to the fact that both shock velocity and the velocity of the leading edge of the rarefaction increase with increasing pressure.

If the flyer plate is thicker than the target and a momentum trap is not used, the pressure pulse duration at the impact plane is determined by the combined transit time of shock and rarefaction waves through the target thickness. At the rear surface of the

target, the duration will be zero.

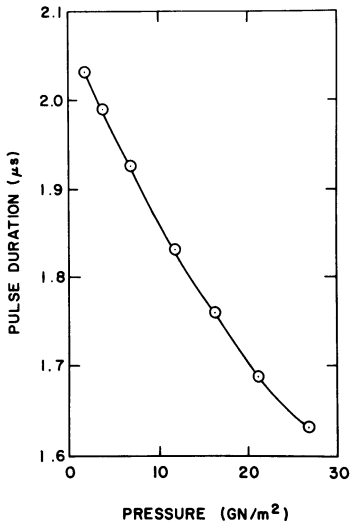

FIGURE 20. Effect of pressure on pulse duration, for a constant flyer-plate thickness (13).

3. Calculation of rarefaction and attenuation rates.

The rarefaction rate, also called release rate, is the slope of the region of the wave in which the decompression is taking place. The tail of the curve has a slope, which varies with pressure and as the wave advances into the target. Figure 15 (b) shows how this rate is dependent upon both pressure and position. The attenuation rate, also called decay rate, measures the rate at which the pressure pulse decreases in amplitude as it travels through the target. The dissipative mechanisms associated with the passage of the pressure pulse are responsible for a steady decrease in the energy carried by it. This reflects itself initially in the decrease of the peak pressure after the pulse duration has been decreased to zero.

Both the rarefaction and attenuation rates can be calculated assuming a hydrodynamic response of the target and flyer plate (Rankine-Hugoniot relations). However, these calculations are only preliminary estimates and have been shown to be significantly different from measured values. As a result, more sophisticated calculational procedures have been developed. This material

transcends the scope of this paper; some additional information is provided in Appendix G (p.1079,this volume).

E. Calculation of Flyer Plate-Target Stand-Off

As indicated in Section IV.C., the Gurney equation does not describe the acceleration history at the flyer plate. It is important to ensure that the flyer plate has reached (or closely approached) its steady-state velocity prior to impact. There are two important considerations that will help to establish the stand-off distance; they will be discussed sequentially, and then a simple semi-empyrical equation for the stand-off distance will be presented.

First, one has the acceleration of the plate from its initial rest position, driven by the expanding detonation products. This problem was treated by Aziz, et al., (14) using a finite difference method.Their results can be applied with some modifications, to flyer plates. The m/c (plate mass/explosive mass) for which Aziz, et al., (14) provide a solution is above the ratios usually encountered in shock loading; one to ten. In order to apply the solution to the lower range of m/c ratios, a cross-plot of Aziz, et al., (14), Figure 4 was made; it is shown in Figure 21 (a). The dashed portions of the plot are extrapolated values. The ordinates express the ratio between the instantaneous and the terminal flyer plate velocities; the various curves apply to different scaled time intervals after the start of the flyer plate motion (Dt/L, where D is the detonation velocity, t is the time, and L the explosive charge thickness). For a value of 0.341, for example, one obtains the curve of Figure 21 (b), in which the scaled time Dt/L is plotted against the ratio between instantaneous and terminal flyer plate velocity. Figure 22 shows how the master plot (for one value of m/c) in Figure 21 (b) can be used for different flyer-plate thicknesses. The velocity approaches the final value assymptotically; hence a cut-off value is taken at 95 pct of the terminal value. This is a good value, because the air drag in the flyer plate target interval effectively slows down the plate somewhat, impeding it from reaching the terminal value. The area under the velocity-time plot is cross-hatched; this area has the units of distance and represents the stand-off. These areas are, for the example shown in Figure 20 equals to 2.2, 4.2, and 17 mm for the 3.18, 6.36, and 25.44 mm flyer plates. These are the minimum stand-off distances. It is readily seen that the thicker plates have lower accelerations. A similar procedure can be followed for any m/c ratio. It should be noticed that Aziz, et al., calculations were applied with the adiabatic exponent equal to 3. This coefficient is a characteristic of the explosive (it usually varies between 2.5 and 3.5) and is described in greater detail in Appendix A (p.1033,this volume).

The second consideration in the flyer plate is the generation of shock waves within it by the detonation of the explosive in its

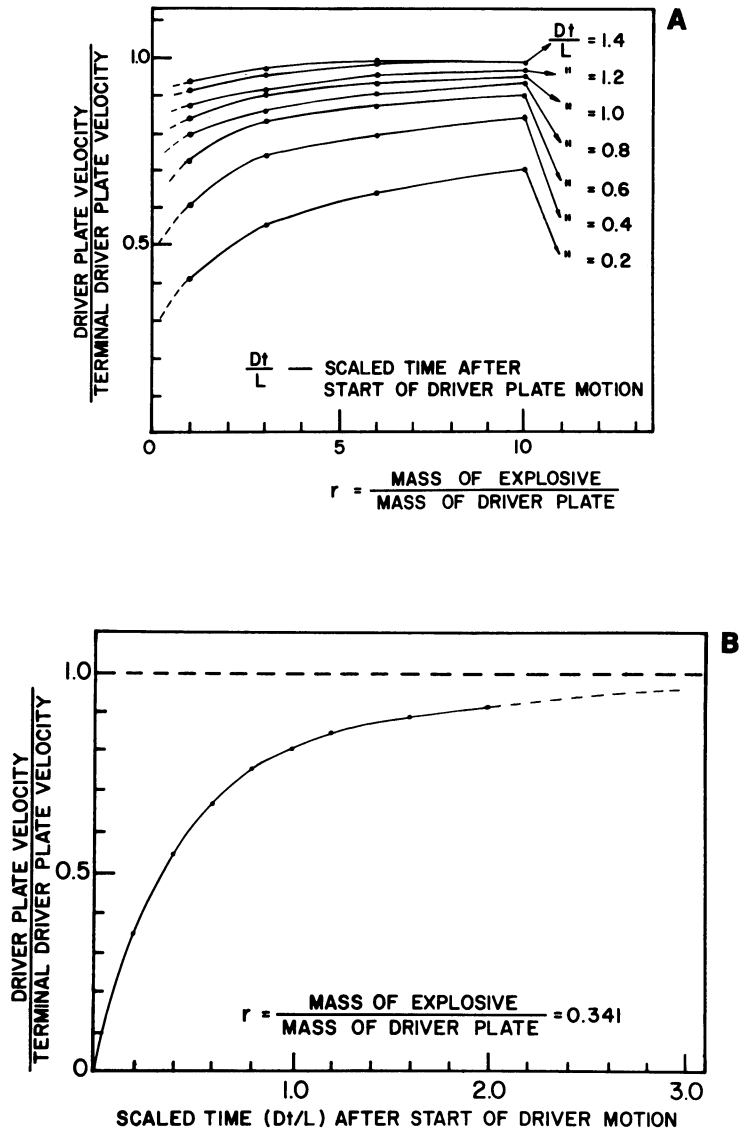

FIGURE 21. (a) Master plot for acceleration of flyer-plate; (25) extrapolated from reference (14)., (b) Scaled time vs. scaled velocity plot obtained from cross-plotting (a).

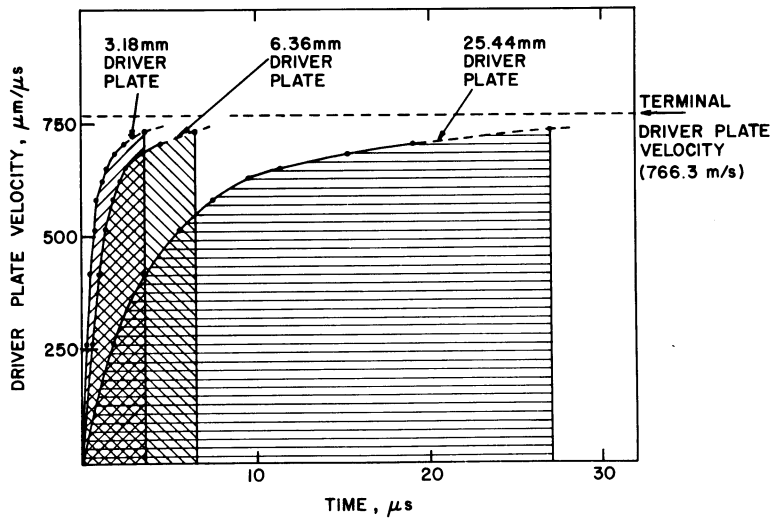

FIGURE 22. Driver-plate velocity vs. time for three different driver-plate thicknesses. Area under curves provides required distance (25).

back surface. One has a situation similar to the one used in contact operations. Figure 23 (a) shows this situation which can be analysed in the x-t plot of Figure 23 (b). The plate only starts to move when the transmitted shock wave reaches the surface opposite to the explosive. It is then reflected back as a rarefaction wave, returning again as a compressive wave when reflected at the detonation side. Upon reaching the opposite surface, it once more accelerates the plate. Figure 23 (c) shows a computer simulation (Normal Initiation Program - NIP) of the first moments of the movement of the front face of the flyer plate (15). The velocity is characterized by steep discontinuities. These discontinuities decrease in amplitude as the wave attenuates itself. After a few reflections the effect can be neglected. Consequently, the true picture of an accelerating flyer plate would be gradually decreasing serrations superimposed on the plots of Figure 22. The shock-reflection effects could produce the spalling of the flyer plate if its thickness is larger than the duration of the pressure pulse generated by the explosive. This would happen at very large m/c ratios. In order to overcome both the velocity discontinuities and possible serrations, a damper material can be used between the explosive and the flyer plate. Materials that have successfully been used for that purpose are 1-5 mm thick lucite sheets, neoprene

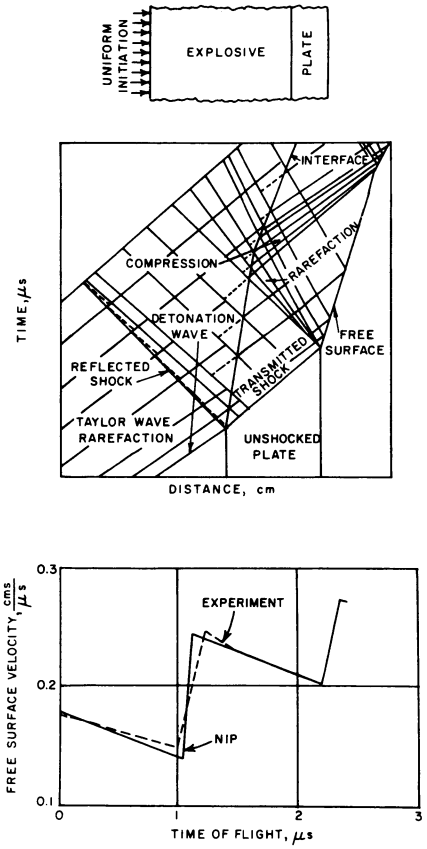

FIGURE 23. Propagation of shock wave from explosive into plate and its acceleration towards a steady-state velocity; successive reflections produce velocity discontinuities (after ref. 15).

foam or, more simply, an air gap. In these cases the mass of the damper material has to be added to the mass of the plate in the m/c computation.

The semi-empirical formula recommended to calculate the stand-off, x , is the following:

$$\frac{x}{V_p} = \frac{10\ t^F}{U_s}$$

This effectively allows the shock wave to reverberate several times in the flyer plate before impact.

F. Momentum Trap-Sample Relationships

As we have mentioned earlier, it is important to perform shock-loading experiments in which the conditions to which a specimen is subjected can be well characterized. Fortunately, the loading history of uniaxial strain, most amenable to analysis, is readily achieved in explosive experiments. One need only take care to eliminate the effects of waves originating at boundaries and interfaces.

The simple flyer plate geometries illustrated in Figures 16 (a) and (b) yield relatively plane impacts over their central regions. The specimen area should therefore lie well within this planar region so that the release waves from the rear of the flyer plate will reach the specimen before lateral release waves reach the specimen-lateral momentum trap interfaces. The specimen should be thin enough that the shock can propagate through the specimen (and cover plate) before arrival of the head of the rarefactions from the rear of the flyer plate. For example, in the system illustrated in Figure 16 (b), the flyer plate could have dimensions of 15 cm x 15 cm by 0.3 cm thick. Appropriate dimensions for the specimen would be 5 cm diameter by 1.2 cm thick, with a 0.15 cm thick cover plate. The anvil thickness could be between 0.5 and 1.5 cm thick; a thickness of 1.5 cm would be adequate for the spall plate. A flyer plate stand-off of about 0.9 cm, three times the flyer plate thickness, would be adequate.

These assembly dimensions can be scaled up or down as desired. The ratio of flyer plate to specimen + cover plate thickness that we have given, 1:5, will in most cases be adequate to insure constant peak pressure through the specimen thickness, provided that flyer and specimen are either the same material or closely matched in shock properties. However, the pressure, pulse duration, and attenuation rate will vary through the specimen thickness.

It is important that all interfaces between metal parts be a very good fit; otherwise, the interfaces will become sources of rarefactions that can propagate into the sample. Ideally, the interfaces will be ground and lapped so that they can be wrung together like gage blocks. All metal parts, i.e., sample, cover plate, anvil, and lateral momentum traps should be either of the same material or should be very closely matched in both density and shock impedance. Additionally, analysis of the pressure history of the sample is much simplified if both flyer plate and sample are either of the same material or are very closely matched in shock impedance.

One simple way of checking the quality of the experimental assembly is to measure the dimensions of the sample before and after shock loading. If these dimensions are relatively unchanged,

one has good evidence that the loading history of the sample was predominantly uniaxial compression and release and that triaxial effects were insignificant.

G. Instrumentation

Instrumentation has been widely used in the past to characterize shock pulses. The techniques used are described in detail in the papers by Fowles (15), Graham and Asay (16), and Taylor (17).

If desired, the simple recovery geometry described in Section IV.F., can be instrumented without seriously perturbing the stress pulse transmitted to the sample. Shorting pins can be placed in the lateral momentum traps and used to measure both impact velocity and impact planarity of the flyer plate. The complete stress history can be monitored via manganin stress gages located in the cover plate and in the anvil above and below the sample. In principle, shorting pin and manganin gage systems are very simple; in practice, even experienced experimenters often fail to obtain meaningful data from an experiment. Hsu, et al. (18) describe the experimental set-up used with manganin piezoresistive gages, as well as some of the results. We therefore suggest that those who wish to begin performing instrumented recovery experiments might best begin by arranging a visit to one or more laboratories in which such experiments are routinely performed.

V. TEMPERATURE EFFECTS

Different thermal effects are associated with the passage of a shock wave. These effects are important enough to warrant careful consideration; they can produce recovery, recrystallization, shear bands, localized melting, reorganization of the dislocation substructure, post-shock aging. Assuming that the shock wave traverses a medium obeying hydrodynamic laws (no shear strength) the temperature rise during the shock pulse can be calculated from the Rankine-Hugoniot relationships. These temperature rises are listed in Appendix B (p.1041,this volume). Upon return to atmospheric pressure, the irreversibility of the process causes the residual temperature to be higher than the initial temperature. An inspection of Appendix B will show that the residual temperature rise is only a fraction of the in-shock temperature rise. The calculated values in Appendix B have been compared to experimentally determined values for copper (19,20), iron (28), stainless steel (21), and aluminum (21). It seems that the measured residual temperatures are, for low pressures, higher than the calculations; for high pressures a better match is obtained, and several investigators have found that the predicted and acutal pressures required for melting are fairly close. One can say that the measured and calculated post-shock temperatures are the same, within a factor of two.

In the impact surface and internal interfaces, on the other hand, additional heating takes place. Urtiew and Grover (22,23) studied this phenomenon and found that surface and interfacial roughness were responsible for temperatures much higher than the ones in the bulk material. Experiments conducted by Meyers, et al (24) confirmed this effect; they found that the impact surface of a shocked sample had a lower hardness than material at 1 mm below the surface, pointing to recovery. Localized melting pockets (known as "hot spots") are often observed on the impact surface, when the projectile-target interface is not exactly planar.

It is thought that internal inhomogeneities, such as voids, second phases, grain boundaries, etc., can give rise to alterations in the wave pattern and attendant temperature rises. Indeed, Leslie, et al. (26) show very clearly how a carbide affects the shock wave. The region at the downstream side of the precipitate (Figure 27 in reference 26) shows a much higher post-shock hardness than the average values.

VI. ACKNOWLEDGMENTS

One of us (M.A.M.) was supported by the National Science Foundation Grant No. DMR-79102 while writing this paper. Appreciation is extended to all members of Denver Research Institute (Denver, Colorado) and Military Institute of Engineering (Rio de Janeiro, Brazil) that were instrumental in the acquisition of the research tools by one of us (M.A.M.).

VII. REFERENCES

1. Huber, G.B., "DuPont Line-Wave Generators", Stanford Research Institute Internal Report No. 040-59, 1959.
2. Kestenbach, H.-J. and Meyers, M.A., *Met. Trans.*, 7A, 1943 (1976).
3. Benedick, W.B., "Detonation Wave Shaping", in "Behavior and Utilization of Explosives in Engineering Design", eds. L. Davidson, et al., New Mexico Section, Albuquerque, N.M., p. 47, 1972.
4. Duvall, G.E., and Fowles, G.R., in "High Pressure Physics and Chemistry", ed. R.S. Bradley, p. 209, vol. 2, Academic Press, New York, 1963.
5. Jones, O.E., "Metal Response Under Explosive Loading", in "Behavior and Utilization of Explosives in Engineering Design", eds. L. Davidson, et al., ASME, New Mexico Section, Albuquerque, N.M., p. 125, 1972.
6. Nordstrom, T.V., Rohde, R.W., and Mottern, D.J., *Met. Trans.*, 6A, 156 (1975).
7. Gurney, R.W., "The Initial Velocities of Fragments From Bombs, Shells, and Grenades," Rep. 405, BRL, Aberdeen Proving Ground, September 14, 1943.

8. Gurney, R.W., "Fragmentation of Bombs, Shells, and Grenades", Rep. 635, BRL, Aberdeen Proving Ground, March 1947.
9. Sterne, T.E., "A Note On The Initial Velocities Of Fragments From Warheads", Rep. 648, BRL, Aberdeen Proving Ground, September, 1947.
10. Henry, I.G., "The Gurney Formula and Related Approximations for the High-Explosive Deployment of Fragments", Report No. PUB-189, Aerospace Group, Hughes Aircraft Comp., California, April, 1967. AD 81 3398.
11. Roth, J., "Correlation of the Gurney Formulae for the Velocity of Explosively-Driven Fragment with the Detonation Parameters of the Driver Plate", Tech. Report 001.71, Poulter Laboratory, Stanford Research Institute, 1971.
12. McQueen, R.G., Marsh, S.P., Taylor, J.W., Fritz, J.N., and Carter, W.J., in "High Velocity Impact Phenomena", ed. R. Kinslow, p. 294, Chapter 7, Academic Press, New York, 1970.
13. Meyers, M.A., *Met. Trans.*, 8A, 1641 (1977).
14. Aziz, A.K., Hurwitz, H., and Sternberg, H.M., *Phys. Fluids*, 4, 380 (1961).
15. Fowles, G.R., in "Dynamic Response of Materials to Intense Impulsive Loading ", eds. Chou, P.C., and Hopkins, A.K., Ch. 8, p. 405, Air Force Materials Lab., W-P.A.F.B., 1972.
16. Graham, R.A., and Asay, J.R., *High Temps.-High Pressures*, 10, 355 (1978).
17. Taylor, J.W., in "Metallurgical Effects at High Strain Rates", eds., Rohde, R.W., Butcher, B.M., Holland, J.R., and Karnes, C.H., p. 107, Plenum Press, N.Y., 1973.
18. Hsu, K.C., Hsu, C.Y., Murr, L.E., and Meyers, M.A., Chapter 27 , this volume.
19. Taylor, J.W., *J.A.P.*, 34, 2727 (1960).
20. Von Holle, W.G., and Trimble, J.J., *J.A.P.*, 47 2391 (1976).
21. Raikes, S.A., and Ahrens, T.J., *Geophys. J.R. Astr. Soc.*, 58, 717 (1979).
22. Urtiew, P.A., and Graver, R., *J.A.P.*, 45, 140 (1974).
23. Grover, R., and Urtiew, P.A., *J.A.P.*, 45, 146 (1974).
24. Meyers, M.A., and Murr, L.E., Chapter 30, this volume.
25. Meyers, M.A., Kestenbach, H-J., and Soares, C.A.O., *Mat. Sci. Eng.*, 45, 143 (1980).
26. Leslie, W.C., Stevens, D.W., and Cohen, M., in "High-Strength Materials", ed. Zackay, V.F., p. 382, John Wiley, New York, 1965.
27. Orava, R.N., and Wittman, R.H., "Techniques for the Control and Application of Explosive Shock Waves", in Proc. 5th Int. Conf., High Energy Rate Fabrication, U. of Denver, Denver, Colorado, p. 1.1.1., 1975.
28. McQueen, R.G., Zukas, E.G., "Residual Temperatures in Shock-Loaded Iron", and Marsh, S.P., ASTM STP No. 336, p. 306, 1962.